



**HAL**  
open science

## Dynamic SIMS for materials analysis in nuclear science

Paula Peres, Seo-Youn Choi, François Desse, Philippe Bienvenu, Ingrid Roure,  
Yves Pipon, Clotilde Gaillard, Nathalie Moncoffre, Lola Sarrasin, Denis  
Mangin

### ► To cite this version:

Paula Peres, Seo-Youn Choi, François Desse, Philippe Bienvenu, Ingrid Roure, et al.. Dynamic SIMS for materials analysis in nuclear science. *J.Vac.Sci.Tech.B*, 2018, 36 (3), pp.03F117. 10.1116/1.5017027 . hal-01959779

**HAL Id: hal-01959779**

**<https://hal.science/hal-01959779>**

Submitted on 21 Dec 2022

**HAL** is a multi-disciplinary open access archive for the deposit and dissemination of scientific research documents, whether they are published or not. The documents may come from teaching and research institutions in France or abroad, or from public or private research centers.

L'archive ouverte pluridisciplinaire **HAL**, est destinée au dépôt et à la diffusion de documents scientifiques de niveau recherche, publiés ou non, émanant des établissements d'enseignement et de recherche français ou étrangers, des laboratoires publics ou privés.

# Dynamic SIMS for materials analysis in nuclear science

Paula Peres,<sup>a)</sup> Seo-Youn Choi, and François Desse  
*CAMECA, 29 quai des Grésillons, 92230 Gennevilliers, France*

Philippe Bienvenu and Ingrid Roure  
*CEA DEN DEC Cadarache, 13108 St Paul Lez Durance, France*

Yves Pipon, Clotilde Gaillard, and Nathalie Moncoffre  
*Université de Lyon, Université Claude Bernard Lyon-1, Institut de Physique Nucléaire de Lyon (IPNL),  
69 622 Villeurbanne, France*

Lola Sarrasin  
*Institut de Physique Nucléaire de Lyon (IPNL), France, Institut de Radioprotection et de Sûreté Nucléaire  
(IRSN), 13115 Cadarache, France*

Denis Mangin  
*Institut Jean Lamour, 54 011 Nancy, France*

(Received 23 November 2017; accepted 7 February 2018; published 26 February 2018)

Offering high sensitivity, depth profiling and ion imaging capabilities together with high throughput, dynamic secondary ion mass spectrometry (SIMS) proves extremely useful for a wide range of nuclear science applications. The CAMECA IMS 7f/7f-Auto is a versatile magnetic sector SIMS well suited for such applications. In this work, various examples of material analyses that are of interest for nuclear science are presented: depth profiling of the xenon and mapping of contaminants in CeO<sub>2</sub>, in-depth distribution of iodine in SiC using the energy filtering technique for improving the I detection limit, and depth profiling analysis of molybdenum in UO<sub>2</sub> using eucentric sample rotation for minimizing surface roughness development (thus improving data quality). *Published by the AVS.* <https://doi.org/10.1116/1.5017027>

## I. INTRODUCTION

When a solid sample is sputtered by primary ions of a few kilo-electron-volt energy, a fraction of the particles emitted from the target is ionized. Secondary ion mass spectrometry (SIMS) consists of analyzing these secondary ions with a mass spectrometer. SIMS is a destructive technique by its nature (sputtering of material) that provides a local analysis of any type of solid material that can be kept under vacuum. SIMS is also recognized as a high sensitivity elemental and isotopic surface analysis technique. While static SIMS focuses on the first top monolayers, providing mostly molecular characterization, dynamic SIMS mode provides bulk composition and in-depth distribution of trace elements with low detection limits.

The dynamic SIMS technique proves extremely useful for a wide range of nuclear science applications: study of fission products behavior in nuclear materials,<sup>1–11</sup> characterization of plasma facing materials in fusion devices,<sup>12–14</sup> investigation of long-term behavior of nuclear materials for safe waste disposal,<sup>15,16</sup> uranium isotope analysis on environmental samples collected from nuclear handling facilities in the search for undeclared nuclear activities,<sup>17–21</sup> and study of uranium accumulation processes in human tissues and cells.<sup>22–24</sup>

Dynamic SIMS is considered to be a major analytical technique for nuclear fuel characterization and is complementary to other techniques used in this field. The first advantage of dynamic SIMS, when compared to electron

probe microanalysis, is its capability to measure the isotopes of fission products and actinides. Other strengths include its high sensitivity (low detection limits) for several elements of interest, including light elements and low yield fission products. Dynamic SIMS also provides high precision isotope ratio measurements, as well as the possibility to directly acquire high depth resolution profiles and/or high resolution ion images in fuel samples. In contrast, the main limitations of SIMS lie in the difficulty to obtain quantitative results, especially in irradiated fuels for which no reference material is available, as well as in the complexity of mass spectra and presence of mass interferences.

The nuclear fuel used in nuclear power reactors is manufactured in rods containing cylindrical UO<sub>2</sub> pellets, or (U, Pu)O<sub>2</sub> in MOx fuel, stacked in a long cladding made of a zirconium-based alloy. During irradiation, the uranium (and plutonium) atoms are transformed by nuclear reaction either into fission products (e.g., Xe, I, Mo...) or other actinides. In addition, the energy produced by fission in the UO<sub>2</sub> ceramic induces a huge thermal gradient in the pellet that strongly affects the chemical behavior of the elements within the ceramic.

For instance, fission noble gases such as xenon can be either “dissolved” in the UO<sub>2</sub> matrix at the position where they were created, in bubbles within the UO<sub>2</sub> ceramic, or released in the gap between the fuel pellet and the cladding. The formation of bubbles induces swelling of the pellet which increases the stress on the inner part of the cladding, potentially creating safety issues. The first study showing that xenon could be measured with SIMS was published by Desgranges and Pasquet.<sup>2</sup> Other studies have proved that

<sup>a)</sup>Electronic mail: paula.peres@ametec.com

xenon atoms filling a bubble can be detected as a peak in a xenon depth profile,<sup>3</sup> which makes possible the determination of the xenon fraction which is located in bubbles or “dissolved” in the UO<sub>2</sub> matrix.<sup>4</sup> Recently, Marchand *et al.*<sup>8</sup> has investigated xenon mobility in UO<sub>2</sub> samples after Xe implantation followed by annealing or irradiation with swift heavy ions.

Several studies have investigated the migration and segregation behavior of other fission products, such as iodine or molybdenum, in UO<sub>2</sub> nuclear fuel.<sup>1</sup> Iodine is a halogen with volatile and corrosive properties susceptible to induce stress corrosion cracking during pellet to cladding interactions. It is thus considered as a key element to be taken into account for safety assessment of nuclear materials. Low detection limits are needed because of the low content level in real samples. Molybdenum is a high yield fission product which presents a complex chemistry, has a low solubility in UO<sub>2</sub>, and is known to affect the behavior of other fission products depending on temperature and partial pressure of oxygen.

The aim of this paper is to illustrate some of the dynamic SIMS applications for the characterization of nuclear fuel, in particular, for the study of diffusion and segregation processes. In order to simulate the chemical behavior of fission products in nuclear fuel, SIMS analyses were performed on different materials after ion implantation with natural isotopes of high fission yield species.

A first study shows how dynamic SIMS can be applied to characterize the xenon noble gas in-depth distribution in a CeO<sub>2</sub> sample. Cerium dioxide (CeO<sub>2</sub>) is usually considered as nonradioactive surrogate of UO<sub>2</sub> ceramics to simulate the properties of nuclear fuels during irradiation processes or long term storage. On this sample, surface mapping of contaminant species has also been obtained.

The second example focuses on the capability of dynamic SIMS to measure iodine at a very low concentration level in a SiC sample. A SiC matrix was selected because of authorization issues with the use of UO<sub>2</sub> in the lab where the analyses were performed. The measurement of <sup>127</sup>I in SiC is challenging because of the several mass interferences that require very high mass resolving power (MRP), not achievable on the instrument. The measurements have been performed using the energy filtering technique in order to remove molecular mass interferences.

In the last study, molybdenum depth profiling measurements were performed in a polycrystalline UO<sub>2</sub> sample. The rotation of the sample during analysis is expected to minimize surface roughness development which is known to occur while sputtering polycrystalline samples.<sup>25</sup> Data obtained without and with eucentric rotation of the sample during analyses are compared.

All measurements shown in this paper were performed using the CAMECA IMS 7f or IMS 7f-Auto, which are magnetic sector mass analyzers dedicated to dynamic SIMS measurements. It should be mentioned that the characterization of highly radioactive samples by dynamic SIMS is possible using specifically designed equipment. A shielded version of the magnetic sector IMS 6f instrument (IMS 6fR) was installed first at CEA Cadarache<sup>26,27</sup> and then at ITU

Karlsruhe for the characterization of irradiated nuclear fuels. This instrument ensures protection of operators and of critical parts of the instrument from contamination and irradiation effects, and it includes additional adaptations to minimize manual operations such as an automatic full-security sample introduction system.

## II. EXPERIMENT

### A. SIMS apparatus

Analyses were performed using the magnetic sector CAMECA IMS 7f or IMS 7f-Auto mass spectrometers. The design of the CAMECA IMS tools is based on a continuous primary ion beam bombardment as well as a continuous secondary ion extraction (DC mode). Two primary ion sources are available, cesium and oxygen, for the analyses of electronegative and electropositive species. Secondary ions are collected using a strong extraction field in order to optimize the instrumental transmission. The CAMECA double focusing mass spectrometer design is based on the coupling of the magnetic sector with an electrostatic sector for efficient mass separation. These instruments work in monocollection mode, secondary ions being acquired one by one by scanning the magnetic field. Two detectors are available, one electron multiplier (EM) for count rates below  $\sim 1 \times 10^6$  counts/s, and one Faraday cup for high counts rates between  $\sim 1 \times 10^6$  and  $\sim 6 \times 10^9$  counts/s.

Different types of SIMS measurements were performed in this study, mostly depth profiling but also mass spectrum and ion imaging analyses. It must be pointed out that because the SIMS technique is destructive, different analyses on the same sample have been performed on different analysis areas.

### B. Xenon and contaminants in CeO<sub>2</sub>

A CeO<sub>2</sub> disk was implanted with xenon (<sup>129</sup>Xe at 220 keV energy, dose  $10^{16}$  at./cm<sup>2</sup>) and then annealed at 1400 °C for 4 h.

Analyses in CeO<sub>2</sub> sample were performed on the CAMECA IMS 7f-Auto using O<sub>2</sub><sup>+</sup> primary ions at 10 keV impact energy and collecting positive secondary ions. A normal incident electron gun was used in order to avoid charging effects during sputtering. Measurements were performed at low mass resolving power and large energy bandwidth (50 or 100 eV).

For depth profiling measurements, the primary current was around 100 nA, the raster size was  $200 \times 200 \mu\text{m}$ , and the analyzed area  $\sim 62 \mu\text{m}$  in diameter. Two analyses were performed: for the first one, both <sup>129</sup>Xe<sup>+</sup> and <sup>140</sup>Ce<sup>+</sup> (matrix) signals were measured, whereas for the second one, only the <sup>129</sup>Xe<sup>+</sup> species was recorded in order to maximize the number of data points per depth unit of the xenon profile. The duration of each depth profile analysis was  $\sim 20$  min.

For scanning ion imaging analyses, a small primary beam size was used in order to optimize the lateral resolution. The primary current was around 120 pA which corresponds to a beam size of  $\sim 1 \mu\text{m}$ . The image field of view, which corresponds to the raster size, was set to  $175 \times 175 \mu\text{m}$ . Ionic images were recorded for <sup>39</sup>K<sup>+</sup>, <sup>138</sup>Ba<sup>+</sup>, <sup>139</sup>La<sup>+</sup> contaminant

species, as well as for the  $^{140}\text{Ce}^+$  matrix species. The total acquisition time for each image was 80 s.

### C. Iodine in SiC

A SiC sample was implanted with iodine ( $^{127}\text{I}$  at 800 keV energy, dose  $10^{11}$  at./cm $^2$ ). Measurements of  $^{127}\text{I}$  implant in SiC sample were performed on the CAMECA IMS 7f-Auto using  $\text{Cs}^+$  primary ions at 15 keV impact energy and collecting negative secondary ions. A normal incident electron gun was used for charge compensation. For all analyses, the primary current was around 100 nA, the raster size was  $125 \times 125 \mu\text{m}$  and the analyzed area  $\sim 62 \mu\text{m}$  in diameter. Measurements were performed at low mass resolving power, energy bandwidth of 30 eV, and for some runs using the energy filtering technique (shift of the energy bandwidth) for removal of mass interferences.

### D. Molybdenum in $\text{UO}_2$

For  $\text{UO}_2$  sample preparation, sintering was first done by AREVA NP at 1750 °C under a reducing atmosphere during 5 h, followed by polishing of the sample surface and annealing of the defects at 1600 °C during 4 h under Ar/5% $\text{H}_2$  atmosphere. Secondary electron microscopy measurements performed after thermal treatment of the surface (1000 °C-10 h) indicated a mean grain size  $\sim 10 \mu\text{m}$ . The samples were implanted with  $^{95}\text{Mo}$  ions at the IMIO 400 accelerator (IPNL, France) at room temperature, using an implantation energy of 400 keV at a fluence of  $10^{16}$  at./cm $^2$ . The expected Mo distribution displays a Gaussian shape with a mean range of 95 nm and a maximum concentration of 0.8 at. %, values calculated using the SRIM-2013 software.<sup>28</sup>

Depth profiling measurements were performed on a CAMECA IMS 7f using  $\text{O}_2^+$  primary bombardment at 5 keV impact energy, and collecting positive secondary ions. The primary current was around 130 nA, the raster size was  $250 \times 250 \mu\text{m}$ , and the analyzed area  $\sim 62 \mu\text{m}$  in diameter. Measurements were performed at low mass resolving power, and the energy bandwidth was set at 100 eV. The instrument was equipped with an eucentric rotating stage; the rotation is eucentric because the axis of rotation coincides with the axis of the mass spectrometer as shown in Fig. 1. Two sets of analyses were performed, without and with rotation of the sample during sputtering (rotation speed of 15 rpm). The duration of a depth profile acquisition was  $\sim 30$  min.

## III. RESULTS AND DISCUSSION

### A. Xenon and contaminants in $\text{CeO}_2$

Figure 2 shows the xenon depth profile obtained in the  $\text{CeO}_2$  sample; an inset provides a zoom of the profile over a selected depth range. The curve shows a baseline signal with a Gaussian in-depth distribution typical of ion implanted species. Interestingly, numerous signal spikes could be detected on top of this baseline signal; these spikes correspond to the numerous peaks observed over the whole depth range. It should be mentioned that similar results were obtained for repeated measurements on different sample

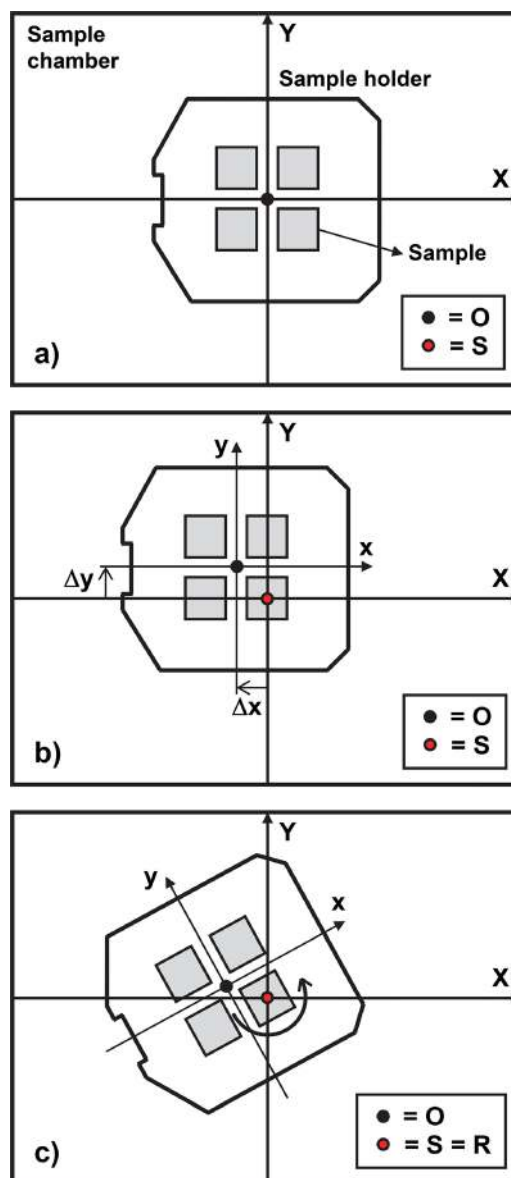


Fig. 1. (Color online) Schematics of the eucentric sample rotation on CAMECA IMS 7f/7f-Auto. (a) Reference position of the sample holder: the sample stage origin O coincides with the axis of the mass spectrometer S; (b) the sample is translated to make the selected analysis point coincide with the mass spectrometer axis S; (c) analysis of the selected analysis point is carried out while rotating, the rotation axis R coincides with the spectrometer axis S.

areas. In addition, the cerium matrix species was recorded together with Xe during a preliminary analysis. A monotonous Ce signal without spikes was observed, which rules out any instrumental issue. Depth calibration was performed by applying a constant sputter rate (SR) over the whole depth profile, obtained from the crater measurement at the end of the analysis using an *ex situ* depth profilometer. This yielded a sputter rate of 39 nm/min. Concentration calibration was performed by imposing the nominal  $^{129}\text{Xe}$  dose value.

The baseline signal corresponds to dissolved Xe, whereas the signal spikes indicate the presence of gas bubbles, expected to have formed during the annealing process. These results are in good agreement with previous studies showing Xe bubble formation in irradiated nuclear fuel.<sup>3,4</sup>

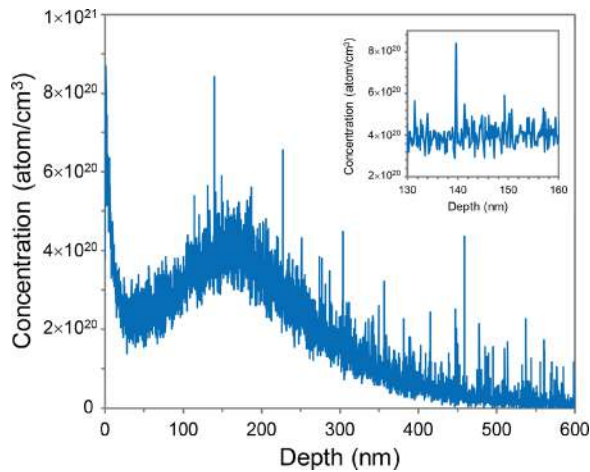


FIG. 2. (Color online) SIMS quantified Xe depth profile obtained in  $^{129}\text{Xe}$  implanted  $\text{CeO}_2$  sample. The inset shows a zoom of the profile over the depth range corresponding to the maximum intensity of the Gaussian base-line distribution.

Xe depth profiling measurements were followed by scanning ion imaging analyses using small primary beam current in order to achieve a lateral resolution of  $\sim 1\ \mu\text{m}$ . Measurements were performed on the sample surface after an initial presputtering using a high beam current ( $\sim 100\ \text{nA}$ ). Data are shown in Fig. 3. On the Ce image, one can distinguish the crystalline contrast of grains due to sputtering rate differences, whereas the ion images for the contaminants show the accumulation of

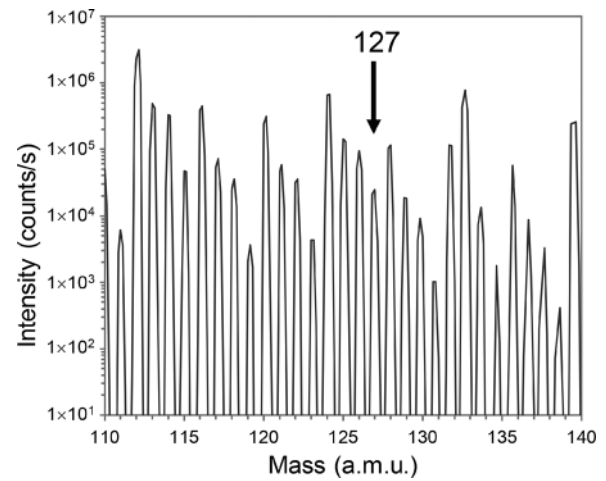


FIG. 4. SIMS mass spectrum recorded in  $^{127}\text{I}$  implanted SiC sample.

impurities as precipitates (K image) or dissolved species at grain boundaries (Ba and La images).

### B. Iodine in SiC

For the SiC sample, a mass spectrum analysis was first performed from 110 to 140 a.m.u. at the near surface of the sample using a widely opened energy slit (100 eV). Data show a complex mass spectrum with a relatively high signal intensity at every mass unit, indicating the presence of mass interferences (Fig. 4). Table I shows the list of computed

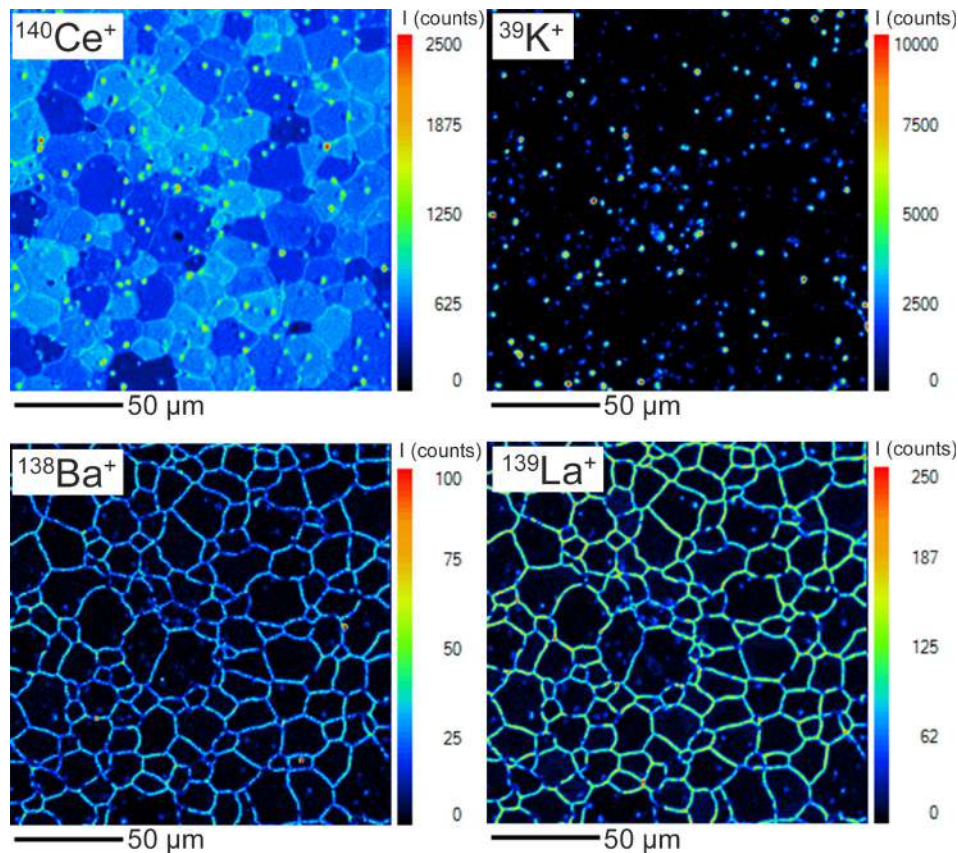


FIG. 3. (Color online) SIMS ion imaging data obtained in  $^{129}\text{Xe}$  implanted  $\text{CeO}_2$  sample for  $^{140}\text{Ce}^+$  matrix species and  $^{39}\text{K}^+$ ,  $^{138}\text{Ba}^+$ ,  $^{139}\text{La}^+$  contaminants. Field of view:  $175 \times 175\ \mu\text{m}^2$ .

TABLE I. List of computed mass interferences near the  $^{127}\text{I}$  mass in a SiC matrix, and corresponding mass resolving power required for separation.

Species	Interferences	MRP
$^{127}\text{I}$	$^{30}\text{Si} \ ^{29}\text{Si} \ ^{28}\text{Si}_2 \ ^{12}\text{C}$	358 487
	$^{30}\text{Si} \ ^{28}\text{Si}_3 \ ^{13}\text{C}$	36 966
	$^{29}\text{Si}_2 \ ^{28}\text{Si}_2 \ ^{13}\text{C}$	22 163
	$^{29}\text{Si}_3 \ ^{28}\text{Si} \ ^{12}\text{C}$	65 448

mass interferences near the mass of  $^{127}\text{I}$  mainly involving the matrix major elements Si and C. Classical high mass resolution conditions cannot be used in this case, as the required MRP values ( $>20\,000$ ) cannot be achieved on the IMS 7f-Auto.

Instead of high mass resolving power conditions, the energy filtering technique was used here for removal of mass interferences at mass 127. The principle of the energy filtering technique is schematically represented in Fig. 5. It is known that the secondary ion energy distribution is narrower

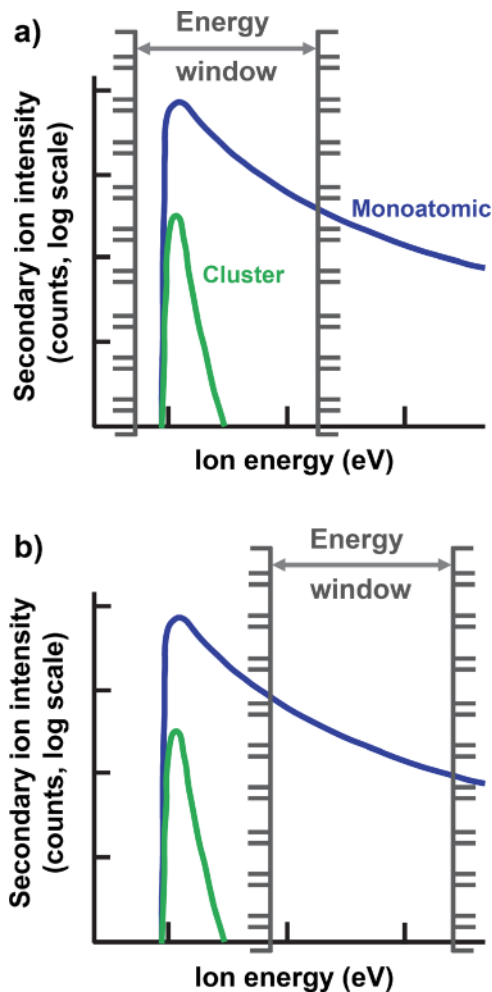


FIG. 5. (Color online) Schematics describing the principle of the energy filtering technique. Energy distribution for monoatomic and cluster (polyatomic) secondary ion species: (a) energy window (or band-pass) centered on the maximum of the energy distribution, (b) energy window translated (by mechanically shifting the energy slit or by applying a sample voltage offset) for removal of cluster mass interferences.

for polyatomic species compared to monoatomic species. By moving the energy band-pass toward the high energy part of the distribution, it is possible to separate monoatomic from isobaric cluster ions; this is the so-called energy filtering technique. The removal of mass interferences using this method requires that the energy distribution of the isotope of interest is sufficiently different from those of the interfering molecular clusters. The principal drawback of this method is the reduced transmission as the energy band-pass is no longer centered on the maximum of the secondary ion energy distribution. In CAMECA IMS magnetic sector instruments, the energy band-pass can be adjusted to any width or position. The width of the energy band-pass is determined by the opening of the energy slit, whereas the position of the energy band-pass can be moved either by applying an offset to the sample voltage or by moving mechanically the energy slit (between  $-130$  and  $+130$  eV for 5 kV sample voltage). The energy slit width and position can be adjusted precisely, and the slit is motorized and computer-controlled in the last CAMECA IMS models.

The energy filtering technique was applied during depth profiling measurements of  $^{127}\text{I}$ . The duration of a depth profiling acquisition varied between  $\sim 17$  and  $\sim 26$  min. In the present case, the energy band-pass was adjusted through the mechanical shift of the energy slit, and not by modifying the

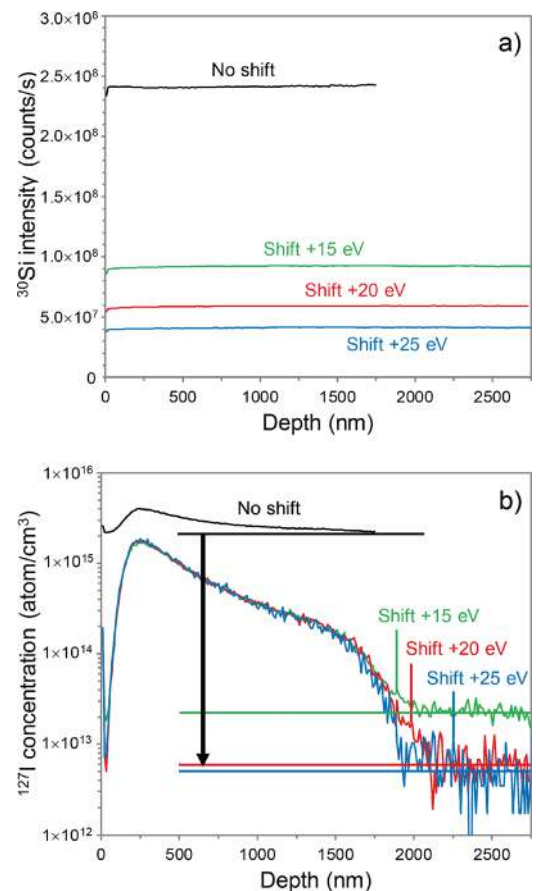


FIG. 6. (Color online) SIMS data obtained in SiC sample for different energy band-pass shifts, raw intensity for  $^{30}\text{Si}$  matrix species (a) and iodine quantified data (b). The black arrow indicates the improvement of detection limit with an energy band-pass shift of  $+20$  eV compared to the data obtained with no shift.

sample voltage since the electron gun had to be used for the analysis of SiC material. In fact, in negative secondary ion extraction mode used for  $I^-$  measurement, the charge neutralization is achieved using a flood of electrons that reaches the sample surface with near-zero energy, which requires the sample voltage to be the same as the electron gun voltage.

Profiles were depth calibrated by applying a constant SR over the whole depth profile. The SR was obtained from the crater measurement performed at the end of the analysis using an *ex situ* depth profilometer. This yielded a sputter rate of  $\sim 106$  nm/min. Concentration calibration was performed by imposing the nominal  $^{127}I$  dose value.

A first depth profile analysis was performed with energy band-pass centered on the maximum of the energy distribution (maximum transmission), then other measurements were performed using different mechanical positions of the energy slit corresponding to a shift toward the high energy of +15, +20, and +25 eV. Different shift values were tested in order to select the conditions corresponding to the higher dynamic

range of the iodine profile (best compromise between removal of mass interferences and instrumental transmission). Figure 6 shows the raw data for the Si matrix species and the quantified data for iodine.

Data obtained for the  $^{30}Si^+$  matrix signal show that there is no loss in data quality when shifting the energy band-pass, as the signal intensity remains stable throughout the whole analysis duration for all measurements independently of the position of the energy band-pass. As expected, the transmission decreases with increasing shift; the transmission for 20 eV shift is approximately four times lower compared to the conditions without shift. However, for the same shift, the background signal due to mass interferences decreases by almost four decades, which results in an improvement of the detection limit of more than three decades.

Data show that the energy filtering technique can be a powerful method for removal of polyatomic mass interferences when analyzing high mass species such as  $^{127}I$ ,

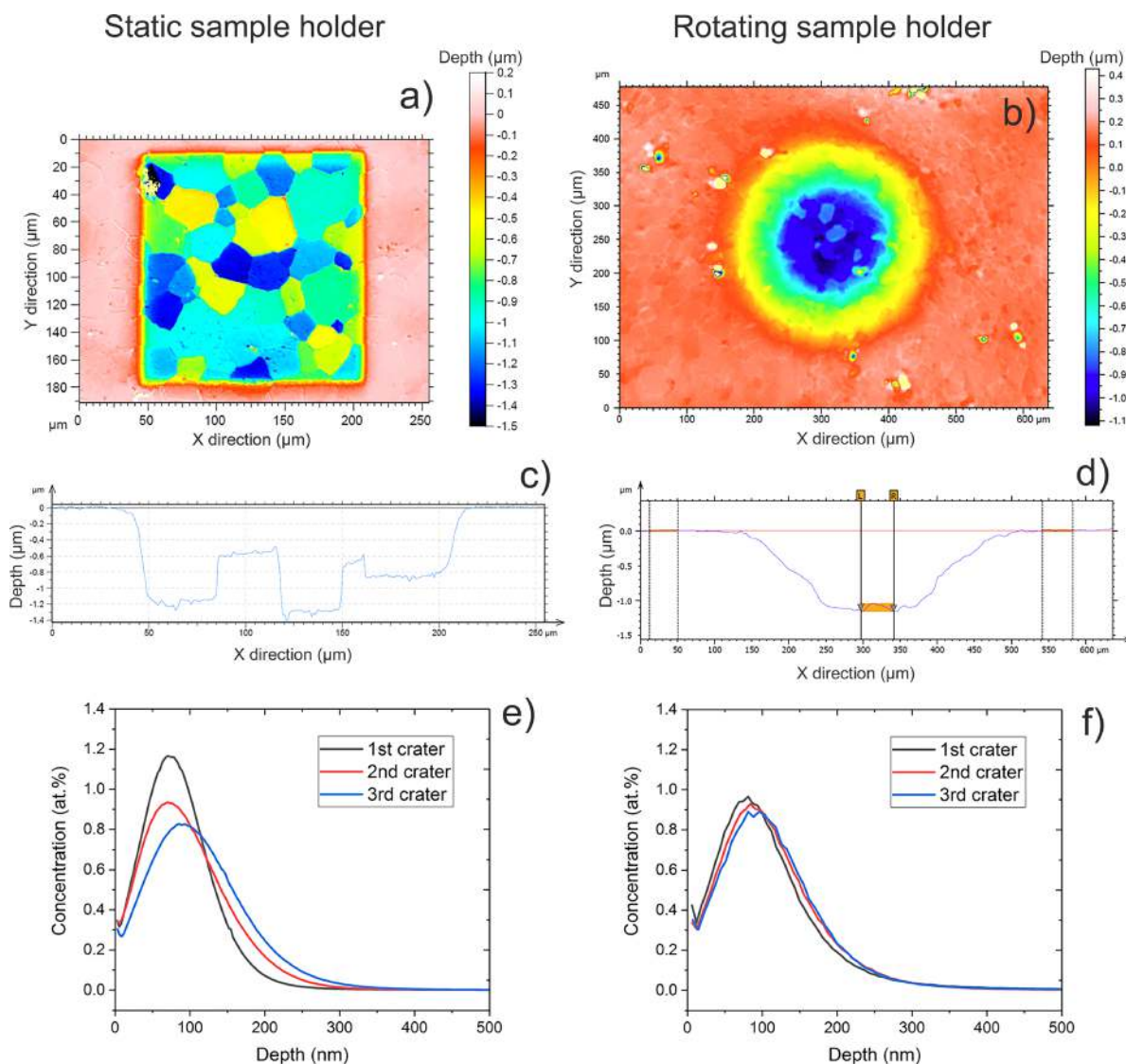


FIG. 7. (Color online) Data obtained in  $UO_2$  polycrystalline sample without (left) and with (right) sample rotation. Crater depth measurements using an optical interferometer [(a) and (b)], linescan obtained from the crater depth measurements [(c) and (d)], and SIMS molybdenum quantified data [(e) and (f)].

resulting in a significant improvement of the depth profile dynamic range and thus of the detection limits.

### C. Molybdenum in UO<sub>2</sub>

The depth calibration of the SIMS profiles was performed using the average crater depth obtained from *ex situ* optical interferometer measurements. The concentration calibration was performed by normalizing the <sup>95</sup>Mo<sup>+</sup> signal to the UO<sup>+</sup> and by applying a relative sensitivity factor (RSF). For each set of measurements, with or without rotation, a RSF value was obtained from a first measurement by imposing the nominal dose value.

The first set of depth profiling measurements in UO<sub>2</sub> sample was performed in static mode (no rotation of the sample during the measurement). Crater depth measurements provided by the optical interferometer have shown the presence of significant roughness at the crater bottom, with ripples of amplitude close to 1 μm [Figs. 7(a) and 7(c)]. Surface roughness development during sputtering is a well-known process that degrades the depth resolution of SIMS measurements. This has been demonstrated for polycrystalline materials like metals so it is likely also to occur in UO<sub>2</sub> polycrystalline samples.<sup>2</sup> One way to inhibit this roughening effect is to rotate the sample while sputtering, so a second set of measurements was performed while rotating the sample during the depth profiling measurements. Crater depth measurements performed after these analyses showed that the crater bottom is significantly flatter, confirming that the sample rotation could efficiently minimize the roughening effects [Figs. 7(b) and 7(d)]. In addition, repeated Mo depth profiling measurements performed without sample rotation show a large scatter of the data with a high variation in the measured dose values [Fig. 7(e)], whereas a much better repeatability between different runs is obtained for measurements performed with sample rotation [Fig. 7(f)].

Data show that eucentric sample rotation during SIMS analyses is an efficient method to minimize surface roughness development in UO<sub>2</sub> polycrystalline samples, thus significantly improving depth profiling data reproducibility.

## IV. SUMMARY AND CONCLUSIONS

To ensure longevity of structural nuclear materials, it is of paramount importance to better understand the diffusion and migration mechanisms of fission products in nuclear fuel. This paper focuses on different applications of dynamic SIMS to the characterization of the in-depth and lateral distribution of trace elements which are of interest in the nuclear reactor operation.

The data shown here illustrate some of the unique analytical advantages of the CAMECA IMS 7f/7f-Auto magnetic sector mass spectrometer design: high sensitivity for achieving low detection limits, depth profiling with high dynamic range, ion imaging with submicrometer resolution, true band-pass energy filter for removal of mass interferences, and rotating stage for minimizing roughness development in polycrystalline samples.

All measurements presented here were performed on ion implanted samples in order to simulate the chemical behavior of fission products in nuclear fuel. Further investigation is likely to focus on the characterization of other Xe implanted CeO<sub>2</sub> samples, with and without an annealing treatment, in order to study in more details the formation of xenon bubbles in nuclear fuels. The next step concerning iodine measurement is to perform similar experiments as those described in this article on a UO<sub>2</sub> matrix or other surrogate material. Additional measurements have been performed using sample rotation on Mo and/or Cs implanted polycrystalline UO<sub>2</sub> samples, in order to study the temperature effect on Mo migration with and without interaction with other fission products such as Cs. Detailed data will be presented in a separate paper.

## ACKNOWLEDGMENTS

The authors would like to thank Philippe Sainsot (INSA Lyon) for the optical interferometer measurements, as well as Roland Ducher and Roland Dubourg (IRSN) for fruitful discussions. The authors are also grateful to Marion Chopin for her assistance in preparing the figures in this paper.

- <sup>1</sup>W. H. Hocking, R. A. Verrall, and I. J. Muir, *J. Nucl. Mater.* **294**, 45 (2001).
- <sup>2</sup>L. Desgranges and B. Pasquet, *Nucl. Instrum. Methods Phys. Res., Sect. B* **215**, 545 (2004).
- <sup>3</sup>J. Lamontagne, J. Noirot, L. Desgranges, T. Blay, B. Pasquet, and I. Roure, *Microchim. Acta* **145**, 91 (2004).
- <sup>4</sup>J. Lamontagne, L. Desgranges, C. Valot, J. Noirot, T. Blay, I. Roure, and B. Pasquet, *Microchim. Acta* **155**, 183 (2006).
- <sup>5</sup>J. Lamontagne, C. Eysseric, L. Desgranges, C. Valot, J. Noirot, T. Blay, I. Roure, and B. Pasquet, *Microchim. Acta* **161**, 355 (2008).
- <sup>6</sup>L. Desgranges, Ch.Valot, and B. Pasquet, *Appl. Surf. Sci.* **252**, 7048 (2006).
- <sup>7</sup>S. Portier, S. Brémier, R. Hasnaoui, O. Bildstein, and C. T. Walker, *Microchim. Acta* **161**, 479 (2008).
- <sup>8</sup>B. Marchand *et al.*, *J. Nucl. Mater.* **440**, 562 (2013).
- <sup>9</sup>J. Lamontagne, Y. Pontillon, E. Esbelin, S. Béjaoui, B. Pasquet, P. Bourdot, and J. M. Bonnerot, *J. Nucl. Mater.* **440**, 366 (2013).
- <sup>10</sup>G. Silbermann *et al.*, *Nucl. Instrum. Methods Phys. Res., B* **332**, 106 (2014).
- <sup>11</sup>T. Zweifel, N. Valle, C. Grygiel, I. Monnet, L. Beck, and W. Petry, *J. Nucl. Mater.* **470**, 251 (2016).
- <sup>12</sup>M. Rubel, J. P. Coad, J. Likonen, V. Philipps, and JET-EFDA Contributors, *Nucl. Instrum. Methods Phys. Res., B* **267**, 711 (2009).
- <sup>13</sup>M. Fukumoto, T. Nakano, K. Masaki, K. Itami, Y. Ueda, and T. Tanabe, *J. Plasma Fusion Res. Ser.* **9**, 369 (2010).
- <sup>14</sup>H. Lefaix-Jeuland, S. Moll, F. Legendre, and F. Jomard, *Nucl. Instrum. Methods Phys. Res., Sect. B* **295**, 69 (2013).
- <sup>15</sup>N. Valle, A. Verney-Carron, J. Sterpenich, G. Libourel, E. Deloule, and P. Jollivet, *Geochim. Cosmochim. Acta* **74**, 3412 (2010).
- <sup>16</sup>A. Verney-Carron *et al.*, *Geochim. Cosmochim. Acta* **203**, 404 (2017).
- <sup>17</sup>Y. Rabeno, P. M. L. Hedberg, M. J. Whitehouse, K. Ingeneri, and S. Littmann, *J. Anal. At. Spectrom.* **24**, 277 (2009).
- <sup>18</sup>P. M. L. Hedberg, P. Peres, J. B. Cliff, F. Rabemananjara, S. Littmann, H. Thiele, C. Vincent, and N. Albert, *J. Anal. At. Spectrom.* **26**, 406 (2011).
- <sup>19</sup>P. Peres, P. M. L. Hedberg, S. Walton, N. Montgomery, J. B. Cliff, F. Rabemananjara, and M. Schuhmacher, *Surf. Interface Anal.* **45**, 561 (2013).
- <sup>20</sup>A.-L. Fauré, C. Rodriguez, O. Marie, J. Aupiais, and F. Pointurier, *J. Anal. At. Spectrom.* **29**, 145 (2014).
- <sup>21</sup>A.-L. Fauré and T. Dalger, *Anal. Chem.* **89**, 6663 (2017).
- <sup>22</sup>C. Tessier, D. Suhard, F. Rebière, M. Soudi, I. Dublineau, and M. Agarande, *Microsc. Microanal.* **18**, 123 (2012).

- <sup>23</sup>C. Poisson, J. Stefani, L. Manens, O. Delissen, D. Suhard, C. Tessier, I. Dublineau, and Y. Guéguen, *Free Radical Res.* **48**, 1218 (2014).
- <sup>24</sup>Y. Guéguen *et al.*, *Toxicol. In Vitro* **30**, 552 (2015).
- <sup>25</sup>R. G. Wilson, F. A. Stevie, and C. W. Magee, *Secondary Ion Mass Spectrometry: A Practical Handbook for Depth Profiling and Bulk Impurity Analysis* (Wiley, New York, 1989).
- <sup>26</sup>B. Rasser, L. Desgranges, and B. Pasquet, *Appl. Surf. Sci.* **203–204**, 673 (2003).
- <sup>27</sup>L. Desgranges and B. Pasquet, *ATALANTE-2004*, Nîmes, France (2004), pp. 1–4.
- <sup>28</sup>J. F. Ziegler, M. D. Ziegler, and J. P. Biersack, *Nucl. Instrum. Methods Phys. Res., Sect. B* **268**, 1818 (2010).